UCRL-13669

STARK BROADENING IN HOT, DENSE LASER-PRODUCED PLASMAS*

Richard J. Tighe and C. F. Hooper, Jr.
Physics Department, University of Florida
Gainesville, Florida 32611

Abstract

Broadened Lyman-α x-ray lines from neon X and argon XVIII radiators, which are immersed in a hot, dense deuterium or deuterium-tritium plasma, are discussed. In particular, these lines are analyzed for several temperature-density cases, characteristic of laser-produced plasmas; special attention paid to the relative importance of ion, electron, and Doppler effects. Static ion microfield distribution functions are tabulated.

*This work was supported in part by the Lawrence Livermore Laboratory, and the Northeast Regional Data Center of the State University System of Florida.

Stark Broadening in Laser-Produced Plasmas

I. Introduction

With the availability of high-powered lasers, it is now possible to produce extremely hot plasmas that are also very dense. Such laser-produced plasmas are currently being studied intensively both in the United States and abroad. An integral part of these investigations is the development of diagnostics for the resulting plasmas. One proposed diagnostic technique would employ x-ray line broadening to determine plasma densities[1]. Experiments on laser-produced plasmas of moderate densities seem to confirm that Stark broadening may be utilized as a diagnostic for high-density laser-produced plasmas[2, 3]. Recently Yaakobi[4] and Burkhalter[5], have both reported the observation of Stark-broadened x-ray lines originating in these dense, hot, laser-produced plasmas.

Some of the experiments being conducted at the Lawrence Livermore Laboratory involve the laser-induced implosion of glass encapsulated deuterium-tritium-gas targets. It has been proposed that these gas targets be seeded with a small amount of higher Z impurity such as neon or argon[6]. Then, for the expected temperature-density conditions produced by the implosion, the D-T plasma would be fully ionized and the impurity would be chosen so that the ion would be hydrogenic. Calculations indicate that some of the Lyman series members of argon XVIII, and possibly also of neon X, will have sufficient intensity to be observed.

In this paper we consider the situation in which a D or D-T gas, seeded with a small percentage of neon or argon, is brought to conditions of temperature-density sufficient to strip a large fraction of the impurity atoms of all but one electron. Under these conditions it should be possible to observe the Lyman series of x-rays. Hence, we will consider Lyman-α radiation from neon X and/or argon XVIII radiators that are immersed in a fully

ionized D or D-T plasma. Our purpose here, in studying the broadening of the Lyman-α line for both hydrogenic neon and argon, is to illustrate how such x-ray lines will be broadened under these extreme conditions. We will analyze these Lyman-alpha lines for various temperature-density cases with special attention paid to the relative importance to the broadening from ion, electron, and Doppler effects. We will then compare our results to those previously found for neutral-hydrogen and ionized-helium radiators immersed in more conventional plasmas.

In section II, we discuss the theoretical formalism: In part II-A we treat the problem of calculating the appropriate electric microfield distribution at a radiator of charge χe. Also in II, especially in II-B we discuss the formalism necessary to combine the static electric microfield contributions with those due to electron and Doppler broadening. In section III we discuss our results, and in IV we present our conclusions together with comments regarding future work.

II. Formalism

The calculations performed herein, are based on a formalism developed in Refs. 7 and 8. In this section we sketch this development, as modified for the case of a hydrogenic, high-Z radiator immersed in a D-T plasma. Following this, we comment on the range of validity of this theory.

For an ion undergoing spontaneous electric-dipole transitions in the presence of a plasma, the intensity distribution of the emitted radiation is given by[9]

$$I(\omega) = \pi^{-1} \mathrm{Re} \int_0^\infty dt\, e^{i\omega t} \left\langle \underset{\sim}{d} \cdot \underset{\sim}{d}(t) \right\rangle \qquad (1)$$

$\langle \ldots \rangle$ indicates an equilibrium average over the states of the entire system consisting of radiator and plasma. $\underset{\sim}{d}$ is the dipole moment operator of the radiating ion, the time dependence of which is generated by the

interactions within the plasma.

Ref. 10 indicates the steps by which Eq. (1) may be written in the form

$$I(\omega) = \int_0^\infty P(\varepsilon)\, J(\omega,\varepsilon)\, d\varepsilon \,. \qquad (2)$$

In this expression, which makes the quasi-static approximation for the ions, $P(\varepsilon)$ is the probability distribution function for the electric microfield due to the static ions. The equilibrium average over the ions is now contained in the microfield integration of Eq. (2). The average over the electrons and the radiator states remains in $J(\omega,\varepsilon)$

$$J(\omega,\varepsilon) = \pi^{-1} \mathrm{Re} \int_0^\infty dt\, e^{i\omega t}\, \mathrm{Tr}_r \left[\underline{d} \cdot \langle \underline{d}(t) \rangle_e \rho^{(r)} \right]. \qquad (3)$$

Tr_r denotes a trace over the internal states of the radiating ion. The heavy brackets represent an average over the electrons only. $\rho^{(r)}$ is the canonical density operator for the radiator given by

$$\rho^{(r)} = \exp(-\beta H_r) / \mathrm{Tr}_r \left[\exp(-\beta H_r) \right]. \qquad (4)$$

After employing a projection-operator technique developed in Ref. 10, and explicitly performing the transform integration in Eq. (3), we obtain the following form for $J(\omega,\varepsilon)$[8]

$$J(\omega,\varepsilon) = -\pi^{-1} \mathrm{Im}\, \mathrm{Tr}_r \left\{ \underline{d} \cdot \left[\Delta\omega - e\underline{\varepsilon} \cdot \underline{R}/\hbar - H(\omega) \right]^{-1} (\rho^{(r)} \underline{d}) \right\} \qquad (5)$$

$\Delta\omega$ is the frequency separation from the unperturbed frequency. The second term in square brackets contains the ion broadening effects; $\underline{R}$ is the position operator for the bound radiator electron. Averaged electron broadening effects appear in the term $H(\omega)$. This result is discussed further in section II-B and in Ref. 8.

The microfield average of Eq. (2) produces the Stark-broadened profile. A final step involves the inclusion of Doppler broadening by a convolution of the Stark profile with a Doppler profile.[9]

$$I(\omega) = \int_{-\infty}^{\infty} I_{\text{Doppler}}(\omega-\omega')\, I_{\text{Stark}}(\omega')\, d\omega', \tag{6}$$

where

$$I_{\text{Doppler}}(\omega) = \frac{Mc^2}{2\pi kT} \exp\left[-\frac{Mc^2}{2kT}\left(\frac{\omega}{\omega_0}\right)^2\right]. \tag{7}$$

M is the mass of the radiating ion and ω_0 is the frequency of the transition in the absence of the plasma:

$$\omega_0 = Z^2\left[\frac{1}{n_2^2} - \frac{1}{n_1^2}\right]. \tag{8}$$

Z is the nuclear charge of the radiator. n_1 and n_2 are the principal quantum numbers for the initial and final levels, respectively, of the transition being studied.

A. Electric Microfield Calculation

The calculation of P(ε) involves the evaluation of the following sine transform,[7, 11]

$$P(\varepsilon) = 2\pi^{-1}\varepsilon\int_0^{\infty} T(l)\sin(\varepsilon l)\, l\, dl \tag{9}$$

where

$$T(l) = Z_N^{-1}\int\cdots\int \exp\left[-\beta V - i\Sigma_j \underset{\sim}{l}_m \cdot \underset{\sim}{\varepsilon}_j\right] d\underset{\sim}{r}_{m1}\cdots d\underset{\sim}{r}_{mN} \tag{10}$$

Z_N is the configurational partition function and β is the inverse temperature, $(kT)^{-1}$. $V = V(\underset{\sim}{r}_1,\ldots,\underset{\sim}{r}_N)$, is the potential energy of the system, including the interaction between the ions and the charged radiator at the origin:

$$V(r_{n1},\cdots,r_{nN})=\sum_{i=1}^{N}\chi\frac{e^2}{r_i}\exp\left(-\frac{r_i}{\lambda_D}\right)+\sum_{i<j}^{N}\frac{e^2}{r_{ij}}\exp\left(-\frac{r_{ij}}{\lambda_D}\right). \tag{11}$$

χe is the charge of the radiator and λ_D is the Debye length,

$$\lambda_D=\left(KT/4\pi ne^2\right)^{1/2}. \tag{12}$$

After introducing the parameters,

$$L=l\epsilon_0\,,\quad a=r_0/\lambda_D,\quad \frac{4}{3}\pi r_0^3 n=1\,, \tag{13}$$

where n is the ion number density, T(L) can be expressed in the form:

$$T(L)=\exp\left[-\gamma L^2+I_1(L)+I_2(L)\right]. \tag{14}$$

The evaluation of γ, $I_1(L)$, and $I_2(L)$ involves the introduction of collective coordinates in performing the multi-dimensional integrations appearing in Eq. (10)[7, 11]; the results are:

$$\gamma=\left[a/4(\alpha^2-2)\right]\left[\alpha^5+2(1-2\sqrt{2})\alpha^4+3\alpha^3+8(\sqrt{2}-1)\alpha^2-6\alpha+4(2-\sqrt{2})\right] \tag{15}$$

$$I_1(L)=3\int dx\,x^2 e^{S(x)}\left[e^{-\beta w_{10}(x)}\left(\frac{\sin(LG(x))}{LG(x)}-1\right)-\left(\frac{\sin(Lq(x))}{Lq(x)}-1\right)\right] \tag{16}$$

where

$$\beta w_{10}(x)=\chi\frac{a^2}{3x}\,e^{-\alpha a x}\,, \tag{17}$$

$$S(x)=\chi\frac{a^3}{3x}\left[\frac{\alpha^2-1}{\alpha^2-2}\right]\left[e^{-\alpha a x}-e^{-\sqrt{2}\alpha x}\right], \tag{18}$$

$$q(x)=-\left[\frac{\alpha^2-1}{\alpha^2-2}\right]\left[\frac{1}{x^2}\left(e^{-\alpha a x}-e^{-\sqrt{2}\alpha x}\right)+\frac{a}{x}\left(\alpha e^{-\alpha a x}-\sqrt{2}\,e^{-\sqrt{2}\alpha x}\right)\right], \tag{19}$$

$$G(x) = q(x) + \frac{1}{x^2} e^{-\alpha a x}(1 + \alpha a x) \qquad (20)$$

α is an effective range parameter the choice of which is well discussed in Refs. 11 and 12. We note here that $P(\varepsilon)$ is essentially parameterized by the two constants $\underline{a}$ and χ.

$$I_2(L) = 3a^2 \sum_k (-1)^k (2k+1)\{\ \}$$

$$\{\ \} = \int_0^\infty x_2^{3/2} I_{k+\frac{1}{2}}(\sqrt{2}a)\, e^{S(x_2)} \left[e^{-\beta w_{10}(x_2)} j_k(LG(x_2)) - j_k(Lq(x_2)) \right]$$

$$\times \int_{x_2}^\infty x_1^{3/2} K_{k+\frac{1}{2}}(\sqrt{2}a)\, e^{S(x_1)} \left[e^{-\beta w_{10}(x_1)} j_k(LG(x_1)) - j_k(Lq(x_1)) \right] dx_1 dx_2$$

$$- \delta_{k,0} \int_0^\infty x_2^{3/2} I_{\frac{1}{2}}(\sqrt{2}a) e^{S(x_2)} \left[e^{-\beta w_{10}(x_2)} - 1 \right]$$

$$\times \int_{x_2}^\infty x_1^{3/2} K_{\frac{1}{2}}(\sqrt{2}a)\, e^{S(x_1)} \left[e^{-\beta w_{10}(x_1)} - 1 \right] dx_1 dx_2 \qquad (21)$$

I and K are modified Bessel functions of the first and third kind. $j_k(\sim)$ is a spherical Bessel function of order k.

Since $I_1(L)$ and $I_2(L)$ are slowly varying functions of L, a table of values for the two functions is computed, from which values of T(L) are produced as needed by interpolation. The asymptotic form for $P(\varepsilon)$ developed in Ref. 7 is used to determine $P(\varepsilon)$ for large values of ε.

B. The Electron Broadening Function, $J(\omega,\varepsilon)$.

The interaction between the radiator and the electron perturbers is assumed to be a point-dipole interaction,

$$V_{int.} = e\underline{R} \cdot \underline{E}_e(\underline{r}) \qquad (22)$$

where $\underset{\sim}{R}$ is the position operator for the bound radiator electron. $\underset{\sim}{\varepsilon}_{\sim e}(r)$ is the electric field, at the position of the radiator, due to an electron perturber located at $\underset{\sim}{r}$. The matrix elements of $\underset{\sim}{R}$ between bound hydrogenic states are proportional to Z^{-1}, thus the interaction V_{int} also scales as Z^{-1}.

As mentioned previously, $J(\omega,\varepsilon)$ can be written in the form,

$$J(\omega,\varepsilon) = -\pi^{-1}\,\mathrm{Im}\,\mathrm{Tr}_r\left\{\underset{\sim}{d}\cdot\left[\Delta\omega - e\underset{\sim}{\varepsilon}\cdot\underset{\sim}{R}/\hbar - H(\omega)\right]^{-1}\left(\rho^{(r)}\underset{\sim}{d}\right)\right\} \quad (5)$$

$[\Delta\omega - e\underset{\sim}{\varepsilon}\cdot\underset{\sim}{R}/\hbar - H(\omega)]^{-1}$ is an effective resolvant operator for the radiator; it is in general a tetradic[10], which operates on the radiator operators to the right of it in equation (5). In the Relaxation Theory formalism $H(\omega)$ is the expanded to second order in V_{int}. The no-quenching approximation, which states that the interaction V_{int} does not induce non-radiative transitions out of the initial excited state of the radiator, is also made. In the case of the Lyman series, where there is no lower-state broadening, the tetradic operator reduces to an ordinary matrix operator[13] whose elements are:

$$\left[\Delta\omega - e\underset{\sim}{\varepsilon}\cdot\underset{\sim}{R}/\hbar - H(\omega)\right]_{\mu\mu'} = \Delta\omega - e\varepsilon R^{z}_{\mu\mu'}/\hbar - H(\omega)_{\mu\mu'} \quad (23)$$

where,

$$H(\omega)_{\mu\mu'} = \hbar^{-2}\Gamma(\Delta\omega)\sum_{\mu''}\underset{\sim}{R}_{\mu\mu''}\cdot\underset{\sim}{R}_{\mu''\mu'} \quad (24)$$

R^z is the z-component of the position operator for the bound radiator electron. The atomic physics of the problem is explicit in the various matrix elements of $\underset{\sim}{R}$. The sum over μ'' runs over the quantum numbers of the upper

level of the desired Lyman transition. In our case, Lyman-α, μ'' runs over the quantum numbers of the n = 2 excited state. It remains to determine Γ(Δω) which contains the average electron broadening effects.

In order to account for the radiator charge, the electron average is carried out using products of Coulomb wave functions for the perturbing electrons. Since electron-electron interactions are neglected in this approach, the perturbers are treated as particles moving independently in the field of the charged radiator. The details of this calculation are given in Ref. 8. The result is

$$\Gamma(\Delta\omega) = -i\left[\frac{4\pi e^4 \lambda_T^3}{3\pi^2}\right] \int_0^\infty\int_0^\infty\int_0^\infty dk_1\, dk_2\, dt$$

$$\times \exp\left[it\left(\Delta\omega + \frac{\hbar k_1^2}{2m} - \frac{\hbar k_2^2}{2m}\right)\right] \exp\left(-\frac{\hbar^2 k_1^2}{2m}\right) f(k_1, k_2) \qquad (25)$$

n is the electron number density, and λ_T is the electron thermal wave length. $k_{\mu 1}$ and k_2 are wave vectors of the perturbing electrons.

$$f(k_1, k_2) = k_1 k_2 \frac{\pi}{2\sqrt{3}}\, g_{ff}(k_1, k_2) \quad , \qquad (26)$$

where g_{ff} is the free-free Gaunt factor discussed by Karzas and Latter[14], and by O'Brien[15].

It is convenient now to separate $\Gamma(\Delta\omega)$ into its real and immaginary parts,

$$\Gamma(\Delta\omega) = \Gamma_{Re}(\Delta\omega) + i\Gamma_{Im}(\Delta\omega)$$

Then it can be shown that[8]

$$\Gamma_{Im}(\Delta\omega>0) = -\left(\frac{2ne^4}{3}\right)\left(\frac{8\pi m}{kT}\right)^{1/2}\left[\frac{2\pi}{\sqrt{3}\theta_R}\right] \times \int_0^\infty \exp\left(-\frac{k_1^2}{\theta_R}\right) k_1 g(k_1,\chi_1)\,dk_1 \tag{27}$$

$$\Gamma_{Im}(\Delta\omega<0) = \exp\left(-|\Delta\omega|/\theta_R\right)\Gamma_{Im}(\Delta\omega>0) \tag{28}$$

$$\Gamma_{Re}(\Delta\omega>0) = \left(\frac{2ne^4}{3}\right)\left(\frac{8\pi m}{kT}\right)^{1/2}\left[\frac{4}{\sqrt{3}\theta_R}\right] \times \int_0^\infty\int_0^\infty \frac{\exp(-k_1^2/\theta_R)\left[k_1k_2 g(k_1,k_2) - k_1\chi_1 g(k_1,\chi_1)\right]}{(\chi_1^2 - k_2^2)}\,dk_1\,dk_2 \tag{29}$$

$$\Gamma_{Re}(\Delta\omega<0)=\left(\frac{2ne^4}{3}\right)\left(\frac{8\pi m}{kT}\right)^{1/2}\left[\frac{4}{\sqrt{3}\,\theta_R}\right]$$

$$\times\int_0^\infty\int_0^\infty \frac{[\exp(-k_1^2/\theta_R)k_1k_2g(k_1,k_2)-\exp(-\chi_2^2/\theta_R)k_2\chi_2g(k_2,\chi_2)]}{(k_1^2-\chi_2^2)}\,dk_1dk_2 \qquad (30)$$

where,

$$\chi_1^2=k_1^2+|\Delta\omega| \quad , \quad \chi_2^2=k_2^2+|\Delta\omega|$$

and θ_R is kT, expressed in Rydberg units.

In the above equations we note that $\Gamma_{Re}(\Delta\omega)$ is expressed in terms of two-dimensional integrals while the expression for $\Gamma_{Im}(\Delta\omega)$ contains only one-dimensional integrals. In Ref. 8 the two-dimensional integrals appearing in Eqs. (29) and (30) were numerically evaluated.

Our present calculational procedure circumvents that necessity by a simplification of Eq. (25). That is, we insert a theta function $\theta(t)$ in Eq. (25) to extend the t-integration from $-\infty$ to $+\infty$. Then, using the integral representation of the theta function, the t- and the k_2- integrations can be performed. In this manner we obtain a dispersion relation expressing $\Gamma_{Re}(\Delta\omega)$ in terms of $\Gamma_{Im}(\Delta\omega)$:

$$\Gamma_{Re}(\Delta\omega)=\pi^{-1}\int_{-\infty}^{\infty}\frac{\Gamma_{Im}(\omega')}{\omega'-\Delta\omega}\,d\omega' \qquad (31)$$

Hence we are able to use the computed values of $\Gamma_{Im}(\Delta\omega)$ in evaluating the one-dimensional integral for $\Gamma_{Re}(\Delta\omega)$. This procedure results in a large reduction in the necessary computer time.

A change of variables in Eq.(27) allows us to compute $\Gamma_{Im}(\Delta\omega)$ rapidly and accurately using Gauss-Laguerre quadrature. Furthermore, since it is a slowly varying function of $\Delta\omega$, a table of values for $\Gamma_{Im}(\Delta\omega)$ is constructed and used to compute numerically the Principal Part integral for $\Gamma_{Re}(\Delta\omega)$.

We have stated above that the electron perturbers move independently of each other and are represented by product wave functions. This implies that $\Gamma_{Im}(\Delta\omega)$ is analogous to the ideal-gas result shown in Fig. 1 of Ref. 16. In order to approximate the effect of electron correlations, we modify (cut off) the functional form of $\Gamma_{Im}(\Delta\omega)$ such that for $\Delta\omega < \omega_p$,

$$\Gamma_{Im}(\Delta\omega < \omega_p) = \Gamma_{Im}(\omega_p) \qquad (32)$$

The effects of this procedure have been discussed in detail in Ref. 16. If we impose the cutoff not at ω_p but at some fraction or multiple thereof, we find that the line center will be lowered or raised. However, the changes are small and quite insensitive to the variation in the cutoff frequency.

Once $\Gamma(\Delta\omega)$ has been computed, Eqs. (23) and (24) are employed in the computation of $J(\omega,\epsilon)$. In the case of Lyman-α, the matrix inversion indicated in Eqs. (5) and (23) may be performed analytically. The details of this matrix inversion and the trace over the states of the upper level of the transition are given in Ref. 13. The result is,

$$J(\omega,\epsilon) = C\,Im\left[\frac{\cosh\left(\frac{3a_0eE}{2kT}\right)(\Delta\omega+3A)+\sinh\left(\frac{3a_0eE}{2kT}\right)\left(\frac{3a_0eE}{2\hbar}\right)}{D}+\frac{2}{\Delta\omega+A}\right] \qquad (33)$$

where $D = (\Delta\omega)^2 + 4\Delta\omega A + 3A^2 - \frac{3aec}{2\hbar}$ and C is a constant which is determined when the area under the line profile is normalized to unity. $A(\Delta\omega)$ is given by,

$$A(\Delta\omega) = -\left(9a_o^2/Z^2\hbar^2\right)\Gamma_{Im}(\Delta\omega) \qquad (34)$$

where a_o is the Bohr radius. The nuclear charge of the radiator, Z, appears explicitly in Eqs. (33) and (34). It is also contained implicitly in $\Gamma(\Delta\omega)$ since the electron perturbers move in the Coulomb field of the hydrogenic radiator of charge $\chi = Z - 1$. That is, the charge of the radiator enters into the computation of the Gaunt factor.

At this point we briefly discuss the range of validity of the second-order theory that we've developed in this section. In dealing with high-temperature ($10^6 - 10^7$ °K) plasmas in the density range, 1×10^{22}/cc – 2×10^{23}/cc, it might be expected that a second-order theory, which is based on the assumption that the vast majority of collisions are weak and which does not include degeneracy effects, would prove invalid. However, it can be shown that for the temperature-density conditions discussed in this paper, degeneracy effects are negligible.[17] To assess the relative strength of the electron interactions for the physical situations considered here, we first note that while the electronic attraction to an ionic radiator of charge Z - 1, is proportional to Z - 1, the binding energy of the bound radiator electron is proportional to Z^2. It follows that the ratio of the energy of such an average electron-radiator interaction to the binding energy of the valence electron is approximately proportional to $n^{1/3}Z^{-1}$; for the worst case considered here, this ratio is approximately 1/10. Another indicator of relative electron-interaction strength that can be discussed is the ratio of the average electron broadening effects to the average energy-level shift of the excited sublevels due to the static-electric-field interaction, $e\underset{\sim}{\mathcal{E}}R/h$ (see. Eq. (23). This ratio is proportional to $\lambda_T/r_o Z$, where λ_T is the thermal wavelength for the electron. Again for cases described in this paper, this ratio will be less than 1/10.

Hence even at the increased densities the assumptions inherent in a second-order theory are valid, at least in the first approximation.

Also, we expect that our theory will be valid inside the plasma frequency, ω_p. Since $\omega_p = 2.72 \times 10^{12} n^{1/2}$ (Rydberg units), we see that as the density increases the second-order theory becomes valid over a larger portion of the line profile.

III. Results

A. Electric Microfield Distribution Functions

In discussing our results we will rely on Figs. 1, 2, 3 and tables I and II.

Figs. 1 and 2 illustrate how the probability-distribution function for finding a given electric field at multiply-charged radiators, immersed in a "gas" of singly-charged ions, changes as a function of the parameter $\underline{a}$. Fig. 3 shows a comparison of the distribution functions for three different values of radiator charge χ at a given value of $\underline{a}$.

From these figures and graphs we observe that the effect on the distribution function when χ is made greater than one, is similar to that which occurs, for $\chi = 1$, when $\underline{a}$ is increased (T is decreased and/or n is increased). That is, as shown in Fig. 3, for $\chi > 1$, the peak of the distribution is shifted to smaller values of ϵ, becomes narrower, and has its maximum value increased.

Furthermore, a comparison of Figs. 1 and 2 (tables I and II) with Fig. 4 (table I) of Ref. 7 reveals that as χ increases the relative sensitivity to changes in $\underline{a}$ increases. This increased sensitivity is due to the fact that in many functions written down in section II-A, the parameter $\underline{a}^2$ is multiplied by χ.

B. Line Profiles

Figs. 4 and 5 show the relative contributions to the Lyman-alpha neon X line profiles from the several broadening mechanisms that are

included in our calculations, together with the combined result. The conditions represented in Fig. 4 correspond to an $\underline{a}$ value of 0.2 while those in Fig. 5 correspond to an $\underline{a}$ value of 0.4. It is clearly seen that the lower the $\underline{a}$ value the broader the ion contribution to the line. The relative importance of the Doppler effect is also of interest. For the temperatures discussed in this paper, the Doppler effect is much more significant - compared to the electron broadening contribution - than was the case when dealing with more conventional plasmas (e.g. $n = 10^{17}$/cc and $T = 40{,}000^{\circ}K$). The qualitative features of the Stark profile are also different: here the electron contribution produces a sharp spike which sits on shoulders provided largely by the ions. Figs. 6 and 7 present plots for argon XVIII that are equivalent to Figs. 4 and 5 for neon X. The qualitative information is the same.

Figs. 8 and 9 show, for neon and argon respectively, families of profiles, each of which corresponds to the same T, but different n. It is evident that as n increases, the profile changes greatly, both in shape and width, thereby illustrating the density sensitivity of the line profile. The practical sensitivity that might be inferred from comparison of experimental and theoretical line shapes depends on at least two factors: 1) how much of the line profile can be experimentally observed, and 2) the resolution of the x-ray spectrometer used.

Figs. 10 and 11 show, that for neon X and argon XVIII, families of three curves, each of which corresponds to the same density, but different T. The results here imply that the frequently mentioned insensitivity of plasma-broadened line profiles to variations in T is significantly reduced as χ increases. The fact that Doppler broadening plays a more significant role in broadening the Argon lines than it does for Neon, is due to the fact that the effect depends not only on mass, but also on the radiator Z.

IV. Summary

The results illustrated, tabulated, and discussed in this paper suggest that the diagnostic potential of plasma-line-broadening which has been clearly demonstrated when applied to conventional plasmas[9, 18], will carry over to laser-produced plasmas where the emitted lines are in the x-ray region. However the decreased temperature insensitivity implies that the use of several series members might better be used to determine the density and to also provide a consistency check on other temperature determinations.

Our deliberations have thus far been based on rather ideal assumptions. We have been assumed that our plasma is optically thin and at a fixed temperature and density. All of these assumptions will break down for the laser-produced plasmas. First, the plasmas are in general optically thick which means that the resonance line can be expected to be greatly altered, over a significant portion of the profile. Hence we are in the process of extending our calculations to higher series members where the effects of optical thickness will be reduced. Secondly, not only will temperature and density not be fixed, but it is expected that the electrons and ions will have different kinetic temperatures. To deal with this problem, we are modifying our theory to allow for different ion and electron kinetic temperatures. Finally, we expect to produce time-averaged profiles, so that we may more realistically analyze experimental data. Toward this end, it should be mentioned that the line profiles illustrated here were very inexpensive to produce - approximately 1/20th the cost of those illustrated in Ref. 8.

We are also in the process of extending our electric microfield and line profile calculation to cases where the radiator has charge Z-1, and the perturbers are hydrogenic (Z-1) and helium-like (Z-2) ions, in varying ratios.

Acknowledgements

We would like to thank Dr. Geoerge F. Chapline of the Lawrence Livermore Laboratory for suggesting this research and Drs. Hugh E. DeWitt (also of LLL) and Robert L. Coldwell (UF) for several helpful discussions.

References

1. A. V. Vinogradov, I. I. Sobel'man, E. A. Yukov, Sov. J. Quant. Electron. 4, 149 (1974).

2. F. E. Irons, J. Phys. B 6, 1562 (1973).

3. V. A. Batanov, V. A. Bogatyrev, N. K. Sukhodrev, and V. B. Fedorov, Sov. Phys. JETP 37, 419 (1973).

4. B. Yaakobi and L. M. Goldman, Bull. Am. Phys. Soc. 20, 1302 (1975).

5. P. G. Burkhalter, Bull. Am. Phys. Soc. 20, 1317 (1975).

6. George F. Chapline, Hugh E. DeWitt, and C. F. Hooper, Jr., UCRL-76272 preprint (1974).

7. John T. O'Brien and C. F. Hooper, Jr., Phys. Rev. A5, 867 (1972).

8. John T. O'Brien and C. F. Hooper, Jr., J. Quant. Spect. Radiat. Transfer 14, 479 (1974).

9. H. R. Griem, Spectral Line Broadening by Plasmas (Academic Press, New York, 1974).

10. E. W. Smith and C. F. Hooper, Jr., Phys. Rev. 157, 126 (1967).

11. C. F. Hooper, Jr., Phys. Rev. 165, 215 (1968).

12. C. F. Hooper, Jr., Phys. Rev. 149, 77 (1966).

13. John T. O'Brien, Ph.D. dissertation, University of Florida (1970).

14. W. J. Karzas and R. Latter, Astrophys. J. Supp. 55, 167 (1961).

15. John T. O'Brien, Astrophys. J., 170, 613 (1971).

16. E. W. Smith, Phys. Rev. 166, 102 (1968).

17. Hugh E. DeWitt, Low-Luminosity Stars, (Gordon and Breach Science Publishers, New York, 1969), Paper III-2.

18. H. R. Griem, Plasma Spectroscopy (McGraw-Hill Book Company, 1964).

Figure Captions

Figure 1: The electric microfield distribution function $P(\varepsilon)$, at a point having a charge of +17. ε is in units of $\varepsilon_0(\varepsilon_0 = e/r_0^2)$ and $a = r_0/\lambda_D$.

Figure 2: The electric microfield distribution function, $P(\varepsilon)$, at a point having a charge of +9. ε is in units of $\varepsilon_0(\varepsilon_0 = e/r_0^2)$ and $a = r_0/\lambda_D$.

Figure 3: Electric microfield distribution functions, $P(\varepsilon)$, for $\underline{a} = 0.6$, at points corresponding to $\chi = 1, 9, 17$. ε is in units of ε_0 $(\varepsilon_0 = e/r_0^2)$ and $\underline{a} = r_0/\lambda_D$.

Figure 4: Line profiles for the Lyman-alpha line of neon X, illustrating various contributions to the complete line profile; a) static ion profile, b) profile including static ions and dynamic electrons, c) profile including static ions, dynamic electrons, and the Doppler effect, d) Doppler profile, $T = 93.9$eV and $n = 1 \times 10^{22}$/cc. $\Delta\omega$ is in units of Rydbergs.

Figure 5: Line profiles for the Lyman-alpha line of neon X, illustrating various contribution to the complete line profile; a) static ion profile, b) profile including static ions and dynamic electrons, c) profile including static ions, dynamic electron and the Doppler effect, d) Doppler profile. $T = 809.1$eV and $n = 1 \times 10^{23}$/cc. $\Delta\omega$ is in units of Rydbergs.

Figure 6: Line profiles for the Lyman-alpha line of Argon XVIII, illustrating various contributions to the complete line profile; a) static ion profile, b) profile including static ions and dynamic electrons, c) profile including static ions, dynamic electrons, and the Doppler effect, d) Doppler profile. $T = 113.2$eV and $n = 2 \times 10^{23}$/cc. $\Delta\omega$ is in units of Rydbergs.

Figure 7: Line profiles for the Lyman-alpha line of Argon XVIII, illustrating various contribution to the complete line profile; a) static ion profile, b) profile including static ions and dynamic electrons, c) profile including static ions, dynamic electrons, and the Doppler effect, d) Doppler profile. $T = 1019.2$eV and $n = 2 \times 10^{23}$/cc. $\Delta\omega$ is in units of Rydbergs.

Figure 8: Neon X Lyman-alpha line profiles, each of which correponds to the same temperature but different density. $\Delta\omega$ is in Rydbergs.

Figure 9: Argon XVIII Lyman-alpha line profiles, each of which corresponds to the same temperature but different density. $\Delta\omega$ is in Rydbergs.

Figure 10: Neon X Lyman-alpha line profiles, each of which corresponds to the same density but different temperature. $\Delta\omega$ is in Rydbergs.

Figure 11: Argon XVIII Lyman-alpha line profiles, each of which corresponds to the same density but different temperature. $\Delta\omega$ is in Rydbergs.

Table Captions

Table I: Probability distributions, $P(\varepsilon)$, at a point having a charge +9 e, for several values of $\underline{a}$. The field strength, ε, is in units of ε_o.

Table II: Probability distributions, $P(\varepsilon)$, at a point having a charge +17 e, for several values of $\underline{a}$. The field strength, ε, is in units of ε_o.

Table I

c	a = 0.2	a = 0.4	a = 0.6	a = 0.8
0.1	0.82795E-02	0.19933E-01	0.50061E-01	0.12237E 00
0.2	0.32355E-01	0.76325E-01	0.18414E 00	0.41742E 00
0.3	0.70015E-01	0.15982E 00	0.36197E 00	0.73441E 00
0.4	0.11793E 00	0.25750E 00	0.53756E 00	0.95661E 00
0.5	0.17206E 00	0.35582E 00	0.67584E 00	0.10474E 01
0.6	0.22817E 00	0.44323E 00	0.76003E 00	0.10281E 01
0.7	0.28227E 00	0.51181E 00	0.78978E 00	0.93966E 00
0.8	0.33099E 00	0.55773E 00	0.77485E 00	0.81936E 00
0.9	0.37184E 00	0.58074E 00	0.72874E 00	0.69277E 00
1.0	0.40329E 00	0.58321E 00	0.66441E 00	0.57426E 00
1.1	0.42471E 00	0.56899E 00	0.59217E 00	0.47032E 00
1.2	0.43629E 00	0.54242E 00	0.51927E 00	0.38264E 00
1.3	0.43883E 00	0.50765E 00	0.45019E 00	0.31040E 00
1.4	0.43352E 00	0.46826E 00	0.38734E 00	0.25178E 00
1.5	0.42178E 00	0.42706E 00	0.33169E 00	0.20455E 00
1.6	0.40507E 00	0.38613E 00	0.28332E 00	0.16669E 00
1.7	0.38481E 00	0.34688E 00	0.24180E 00	0.13636E 00
1.8	0.36224E 00	0.31018E 00	0.20646E 00	0.11204E 00
1.9	0.33844E 00	0.27649E 00	0.17652E 00	0.92505E-01
2.0	0.31427E 00	0.24600E 00	0.15124E 00	0.76738E-01
2.5	0.20551E 00	0.13715E 00	0.72915E-01	0.32482E-01
3.0	0.13116E 00	0.79675E-01	0.38276E-01	0.15390E-01
3.5	0.85068E-01	0.48503E-01	0.21727E-01	0.77776E-02
4.0	0.57464E-01	0.31248E-01	0.13077E-01	0.41504E-02
4.5	0.40516E-01	0.21209E-01	0.81010E-02	0.23258E-02
5.0	0.29671E-01	0.14989E-01	0.51674E-02	0.13616E-02
6.0	0.17142E-01	0.60386E-02	0.22912E-02	0.52827E-03
7.0	0.10789E-01	0.45998E-02	0.11280E-02	0.23564E-03
8.0	0.72993E-02	0.27943E-02	0.61011E-03	0.11756E-03
9.0	0.52370E-02	0.17931E-02	0.35875E-03	0.64287E-04

Table I

10.0	0.39335E-02	0.12092E-02	0.22692E-03	0.37953E-04
12.0	0.24105E-02	0.62569E-03	0.10834E-03	0.15666E-04
14.0	0.15585E-02	0.37178E-03	0.61023E-04	0.73255E-05
16.0	0.10512E-02	0.24365E-03	0.37269E-04	0.35754E-05
18.0	0.73717E-03	0.16914E-03	0.23137E-04	0.18041E-05
20.0	0.53550E-03	0.12035E-03	0.14510E-04	0.93957E-06
22.0	0.40156E-03	0.87183E-04	0.92342E-05	0.50419E-06
24.0	0.30975E-03	0.64236E-04	0.59900E-05	0.27831E-06
26.0	0.24490E-03	0.48092E-04	0.39741E-05	0.15776E-06
28.0	0.19777E-03	0.36551E-04	0.26941E-05	0.91682E-07
30.0	0.16255E-03	0.28174E-04	0.18622E-05	0.54532E-07
35.0	0.10503E-03	0.15539E-04	0.79448E-06	0.16307E-07
40.0	0.71638E-04	0.91622E-05	0.36830E-06	0.54218E-08
45.0	0.50974E-04	0.56849E-05	0.18222E-06	0.19609E-08
50.0	0.37507E-04	0.36742E-05	0.95030E-07	0.75974E-09
60.0	0.21932E-04	0.16876E-05	0.29264E-07	0.13436E-09
70.0	0.13850E-04	0.85331E-06	0.10237E-07	0.28175E-10
80.0	0.92562E-05	0.46362E-06	0.39452E-08	0.67364E-11
90.0	0.64616E-05	0.26642E-06	0.16415E-08	0.17885E-11
100.0	0.46688E-05	0.16013E-06	0.72675E-09	0.51737E-12

Table II

ε	a = 0.2	a = 0.4	a = 0.6	a = 0.8
0.1	0.95228E-02	0.28835E-01	0.87047E-01	0.24017E 00
0.2	0.37158E-01	0.10951E 00	0.31204E 00	0.76925E 00
0.3	0.80215E-01	0.22627E 00	0.58882E 00	0.12320E 01
0.4	0.13465E 00	0.35799E 00	0.82879E 00	0.14314E 01
0.5	0.19562E 00	0.48363E 00	0.97782E 00	0.13816E 01
0.6	0.25808E 00	0.58673E 00	0.10245E 01	0.11891E 01
0.7	0.31738E 00	0.65769E 00	0.98700E 00	0.95200E 00
0.8	0.36968E 00	0.69383E 00	0.89527E 00	0.72853E 00
0.9	0.41225E 00	0.69796E 00	0.77760E 00	0.54282E 00
1.0	0.44355E 00	0.67612E 00	0.65488E 00	0.39835E 00
1.1	0.46313E 00	0.63564E 00	0.53982E 00	0.29057E 00
1.2	0.47149E 00	0.58360E 00	0.43866E 00	0.21173E 00
1.3	0.46980E 00	0.52597E 00	0.35331E 00	0.15468E 00
1.4	0.45964E 00	0.46730E 00	0.28320E 00	0.11377E 00
1.5	0.44278E 00	0.41072E 00	0.22662E 00	0.84086E-01
1.6	0.42099E 00	0.35815E 00	0.18145E 00	0.62798E-01
1.7	0.39590E 00	0.31061E 00	0.14561E 00	0.47238E-01
1.8	0.36892E 00	0.26843E 00	0.11725E 00	0.35784E-01
1.9	0.34122E 00	0.23153E 00	0.94821E-01	0.27502E-01
2.0	0.31371E 00	0.19958E 00	0.77057E-01	0.21122E-01
2.5	0.19583E 00	0.96666E-01	0.29511E-01	0.61281E-02
3.0	0.12025E 00	0.50139E-01	0.12954E-01	0.23034E-02
3.5	0.75688E-01	0.27997E-01	0.65264E-02	0.11119E-02
4.0	0.49866E-01	0.16809E-01	0.37288E-02	0.63823E-03
4.5	0.34268E-01	0.10658E-01	0.23715E-02	0.37731E-03
5.0	0.24542E-01	0.70776E-02	0.15980E-02	0.22775E-03
6.0	0.13796E-01	0.34344E-02	0.74376E-03	0.84627E-04
7.0	0.83781E-02	0.18018E-02	0.35938E-03	0.32703E-04
8.0	0.53663E-02	0.10092E-02	0.18001E-03	0.13126E-04
9.0	0.36029E-02	0.60027E-03	0.93331E-04	0.54647E-05

Table II

10.0	0.25254E-02	0.37715E-03	0.50016E-04	0.23568E-05
12.0	0.13890E-02	0.17178E-03	0.15767E-04	0.48479E-06
14.0	0.86449E-03	0.91379E-04	0.55728E-05	0.11306E-06
16.0	0.58938E-03	0.54402E-04	0.21825E-05	0.29582E-07
18.0	0.42614E-03	0.34735E-04	0.93600E-06	0.85947E-08
20.0	0.31716E-03	0.22793E-04	0.43440E-06	0.27439E-08
22.0	0.24048E-03	0.14962E-04	0.21561E-06	0.95263E-09
24.0	0.18514E-03	0.10010E-04	0.11311E-06	0.35593E-09
26.0	0.14534E-03	0.68513E-05	0.61975E-07	0.14164E-09
28.0	0.11575E-03	0.47876E-05	0.35056E-07	0.59404E-10
30.0	0.93423E-04	0.34090E-05	0.20323E-07	0.25988E-10
35.0	0.57539E-04	0.15630E-05	0.57179E-08	0.5?381E-11
40.0	0.37575E-04	0.77485E-06	0.17985E-08	0.62702E-12
45.0	0.25666E-04	0.40847E-06	0.61783E-09	0.11911E-12
50.0	0.18169E-04	0.22627E-06	0.22812E-09	0.25071E-13
60.0	0.98870E-05	0.78005E-07	0.36929E-10	0.14225E-14
70.0	0.58438E-05	0.30289E-07	0.71466E-11	0.10465E-15
80.0	0.36723E-05	0.12870E-07	0.15868E-11	0.94251E-17
90.0	0.24195E-05	0.58705E-08	0.39320E-12	0.99924E-18
100.0	0.16551E-05	0.28358E-08	0.10660E-12	0.12121E-18

Fig 1.

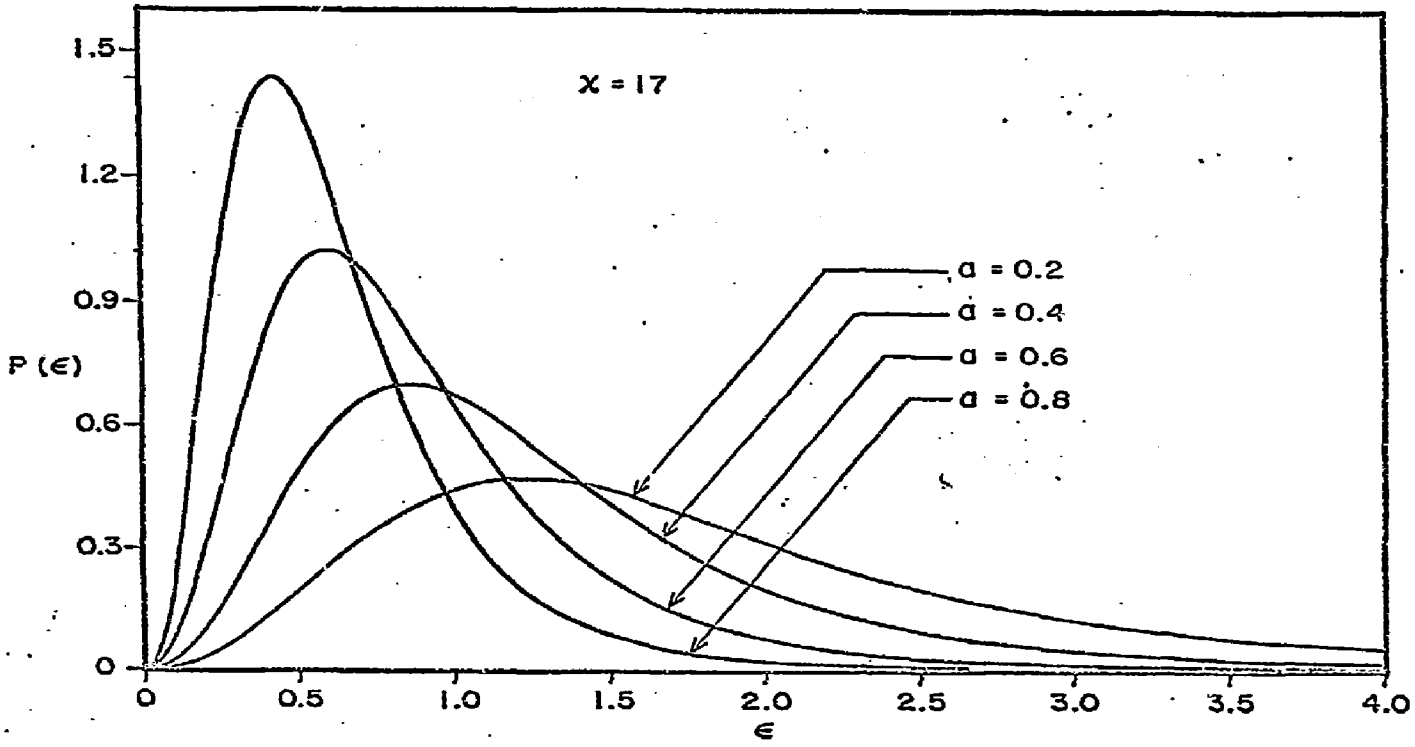

Fig. 2.

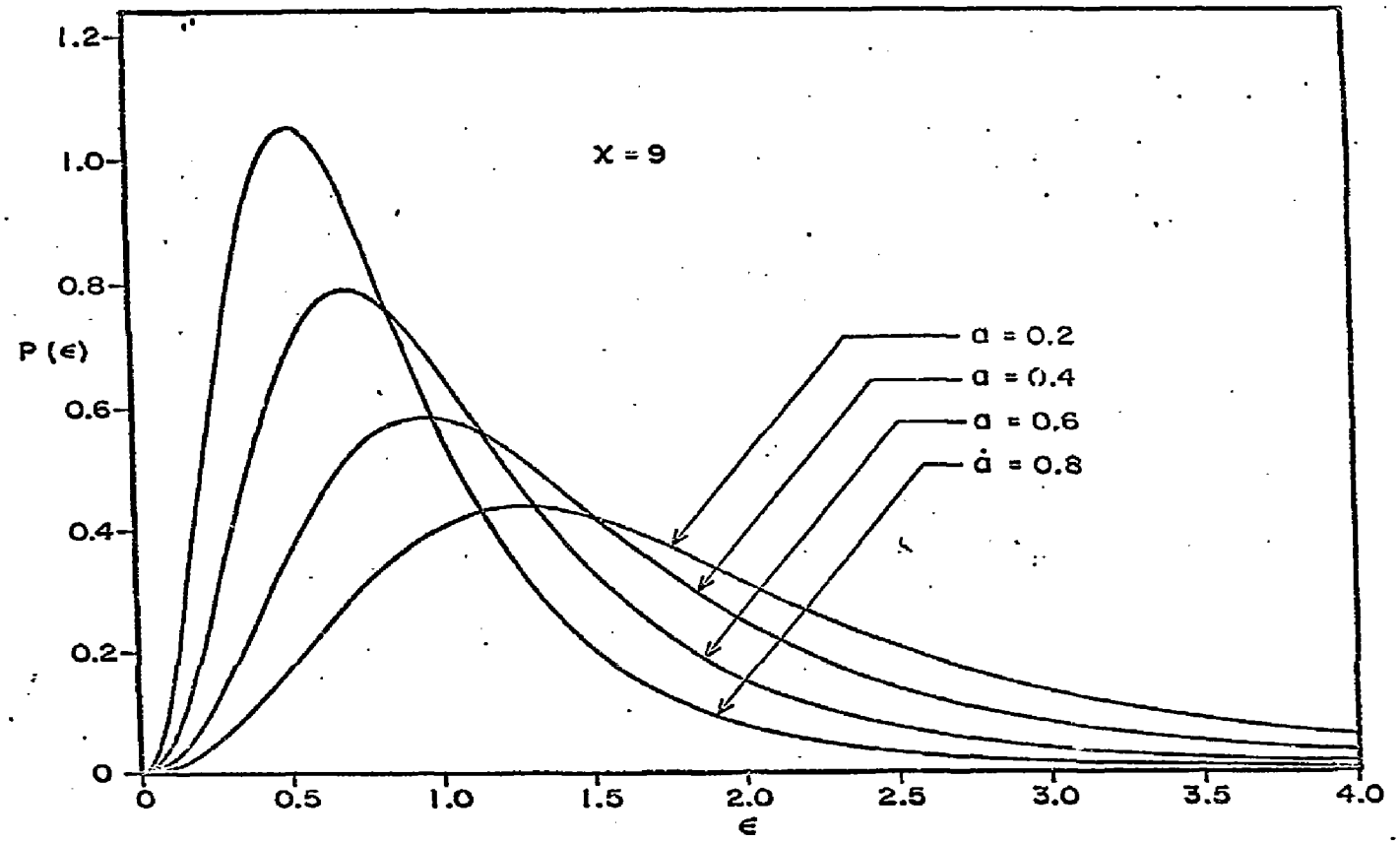

Fig 3

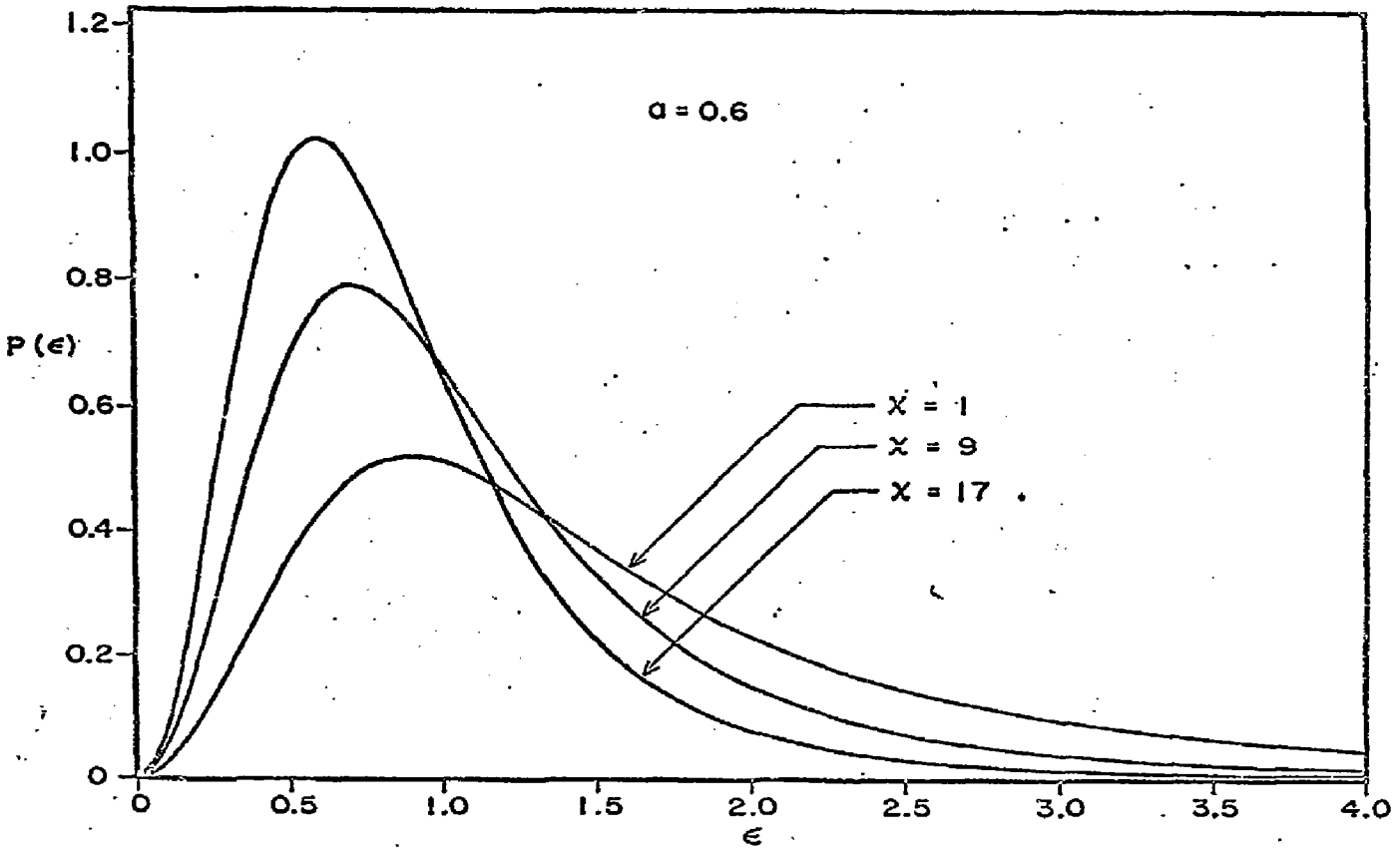

Fig 4

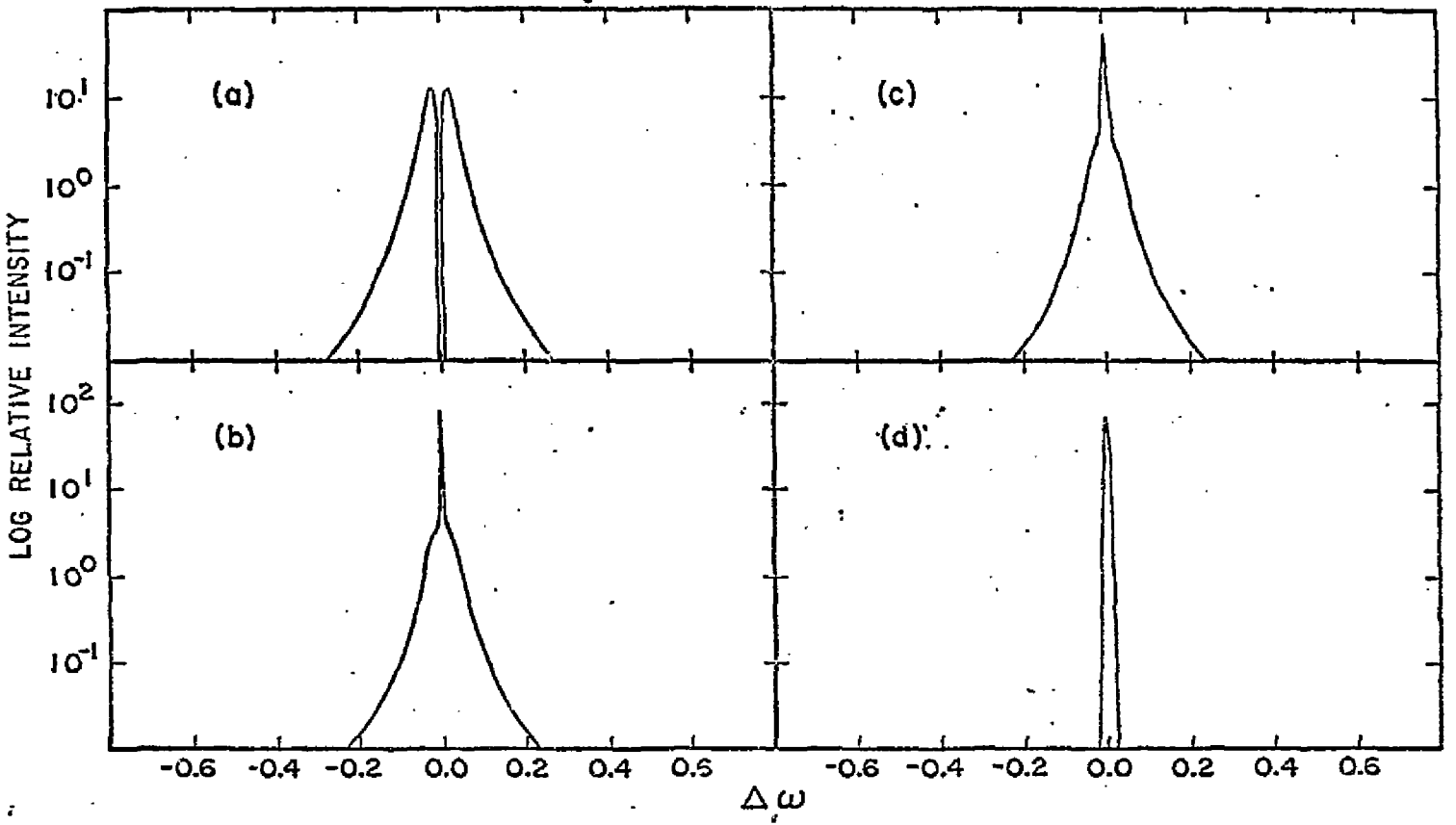
(a)
(b)
(c)
(d)
LOG RELATIVE INTENSITY
10^1
10^0
10^{-1}
10^2
-0.6 -0.4 -0.2 0.0 0.2 0.4 0.6
$\Delta\omega$

Fig 5

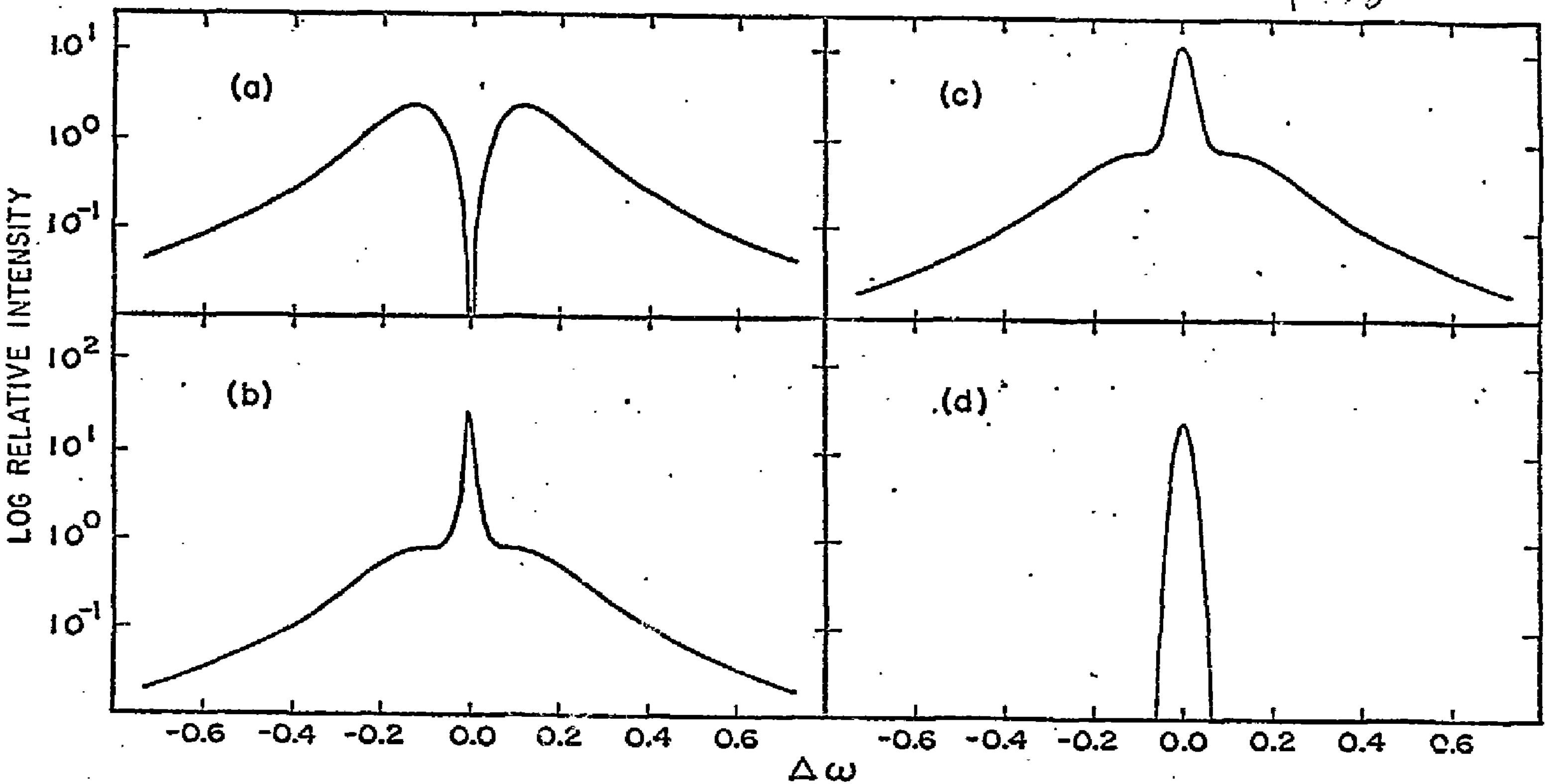
LOG RELATIVE INTENSITY
(a)
(b)
(c)
(d)
10^1
10^0
10^{-1}
10^2
-0.6 -0.4 -0.2 0.0 0.2 0.4 0.6
$\Delta\omega$

Fig 6

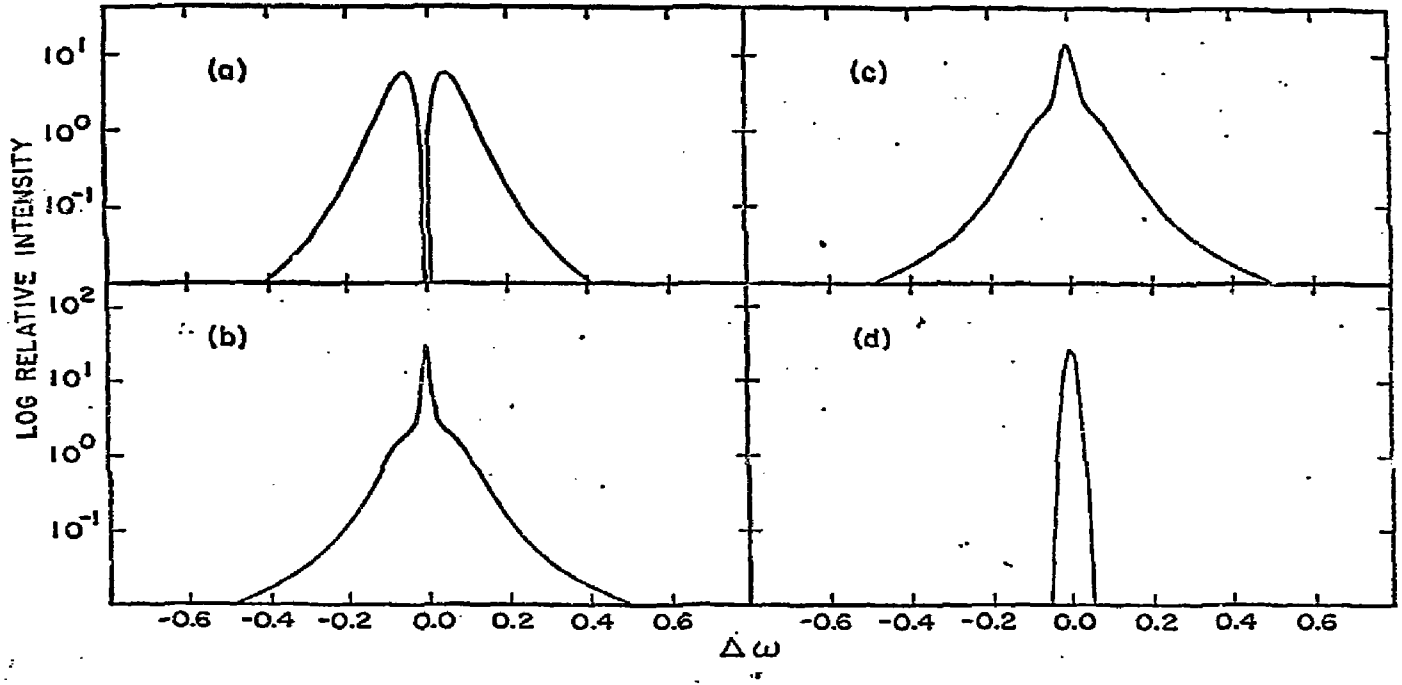
(a)
(b)
(c)
(d)
LOG RELATIVE INTENSITY
10^1
10^0
10^{-1}
10^2
-0.6 -0.4 -0.2 0.0 0.2 0.4 0.6
$\Delta\omega$

Fig 7

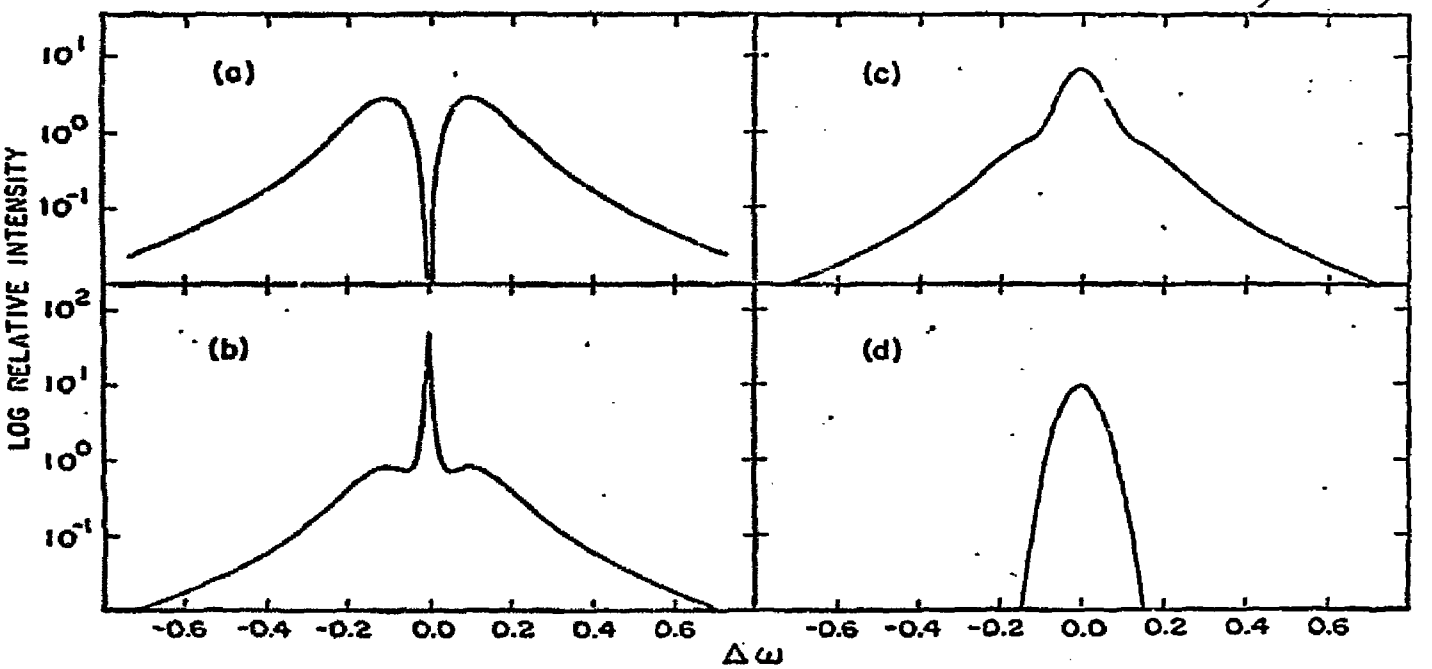
(a)
(b)
(c)
(d)
LOG RELATIVE INTENSITY
10^1
10^0
10^{-1}
10^2
10^1
10^0
10^{-1}
-0.6 -0.4 -0.2 0.0 0.2 0.4 0.6
-0.6 -0.4 -0.2 0.0 0.2 0.4 0.6
$\Delta\omega$

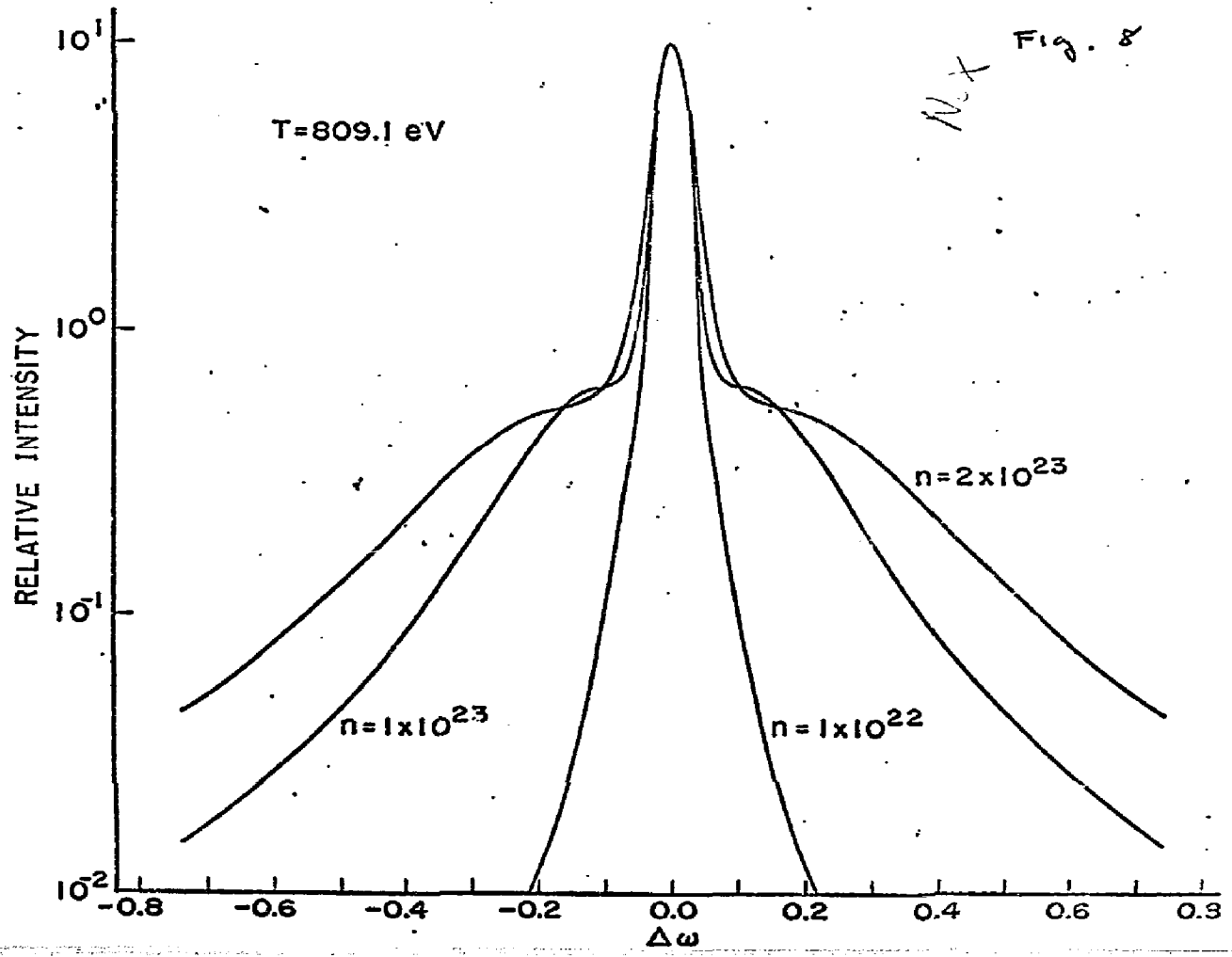
Fig. 8
T=809.1 eV
RELATIVE INTENSITY
10^1
10^0
10^{-1}
10^{-2}
n=2x10^23
n=1x10^23
n=1x10^22
-0.8
-0.6
-0.4
-0.2
0.0
0.2
0.4
0.6
0.8
Δω

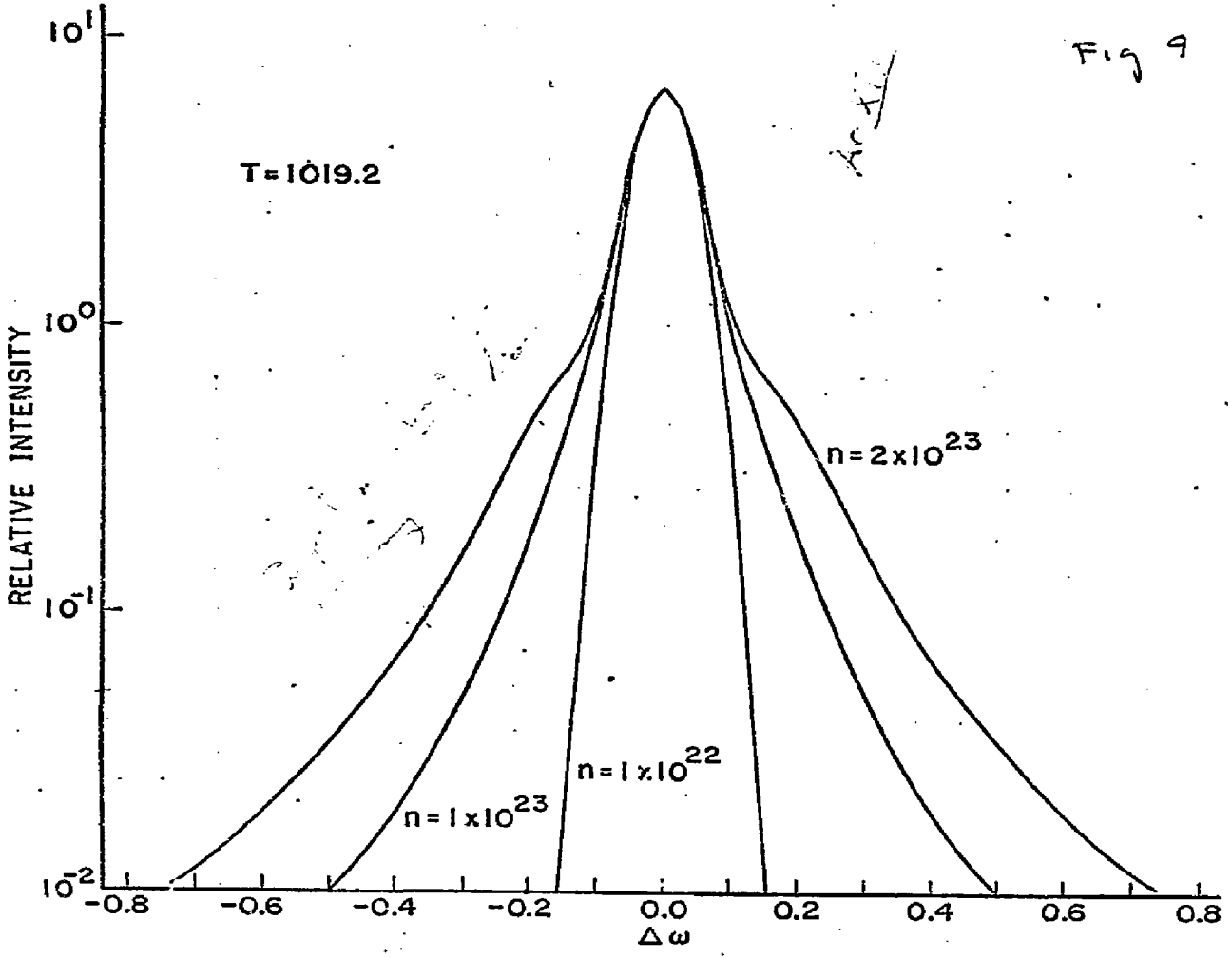
Fig 9
T=1019.2
RELATIVE INTENSITY
10^{1}
10^{0}
10^{-1}
10^{-2}
n=2x10^23
n=1x10^22
n=1x10^23
-0.8
-0.6
-0.4
-0.2
0.0
0.2
0.4
0.6
0.8
Δω

Fig 10

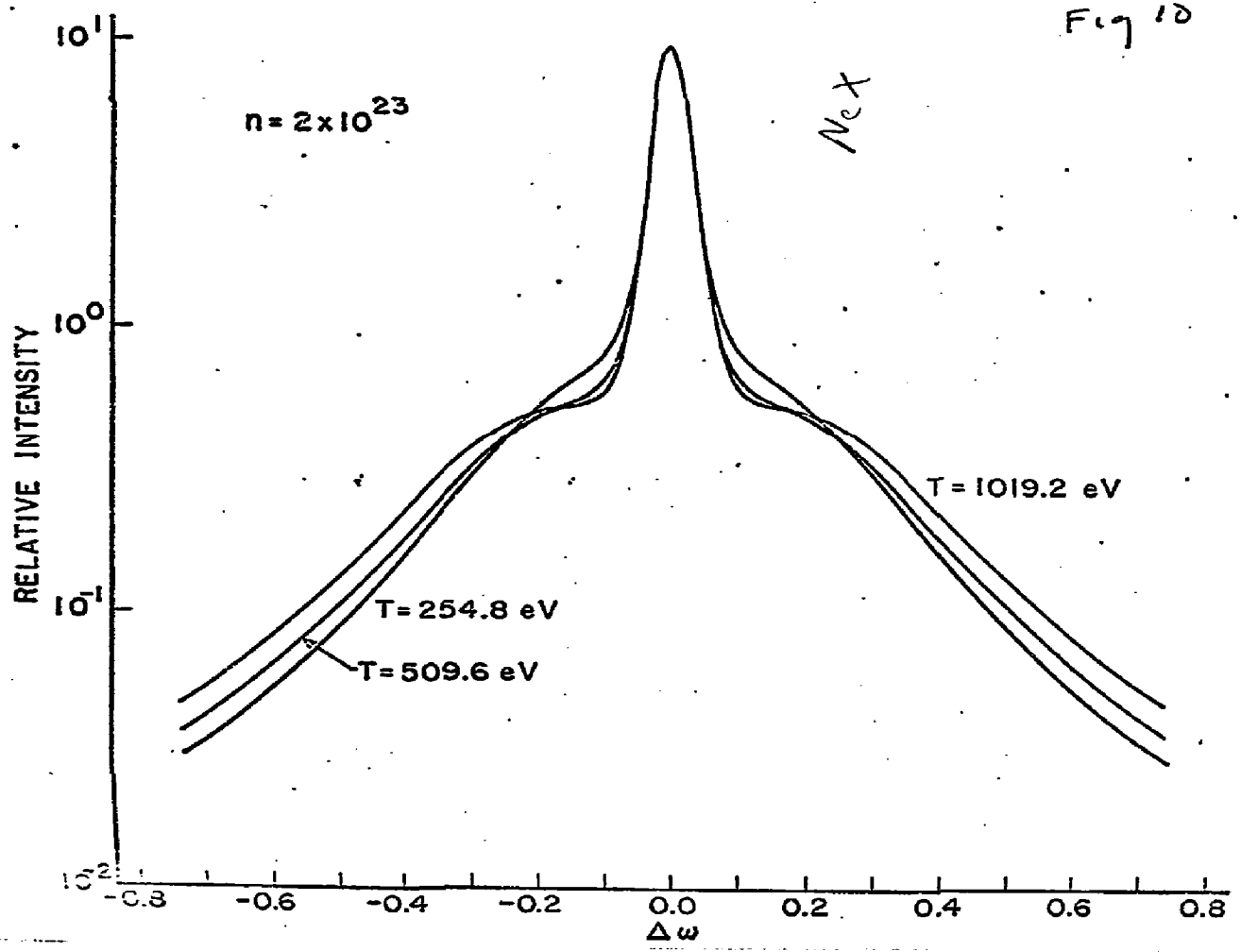
Ne X
n = 2x10^23
RELATIVE INTENSITY
10^1
10^0
10^-1
10^-2
T = 1019.2 eV
T = 254.8 eV
T = 509.6 eV
-0.8
-0.6
-0.4
-0.2
0.0
0.2
0.4
0.6
0.8
Δω

Fig 11

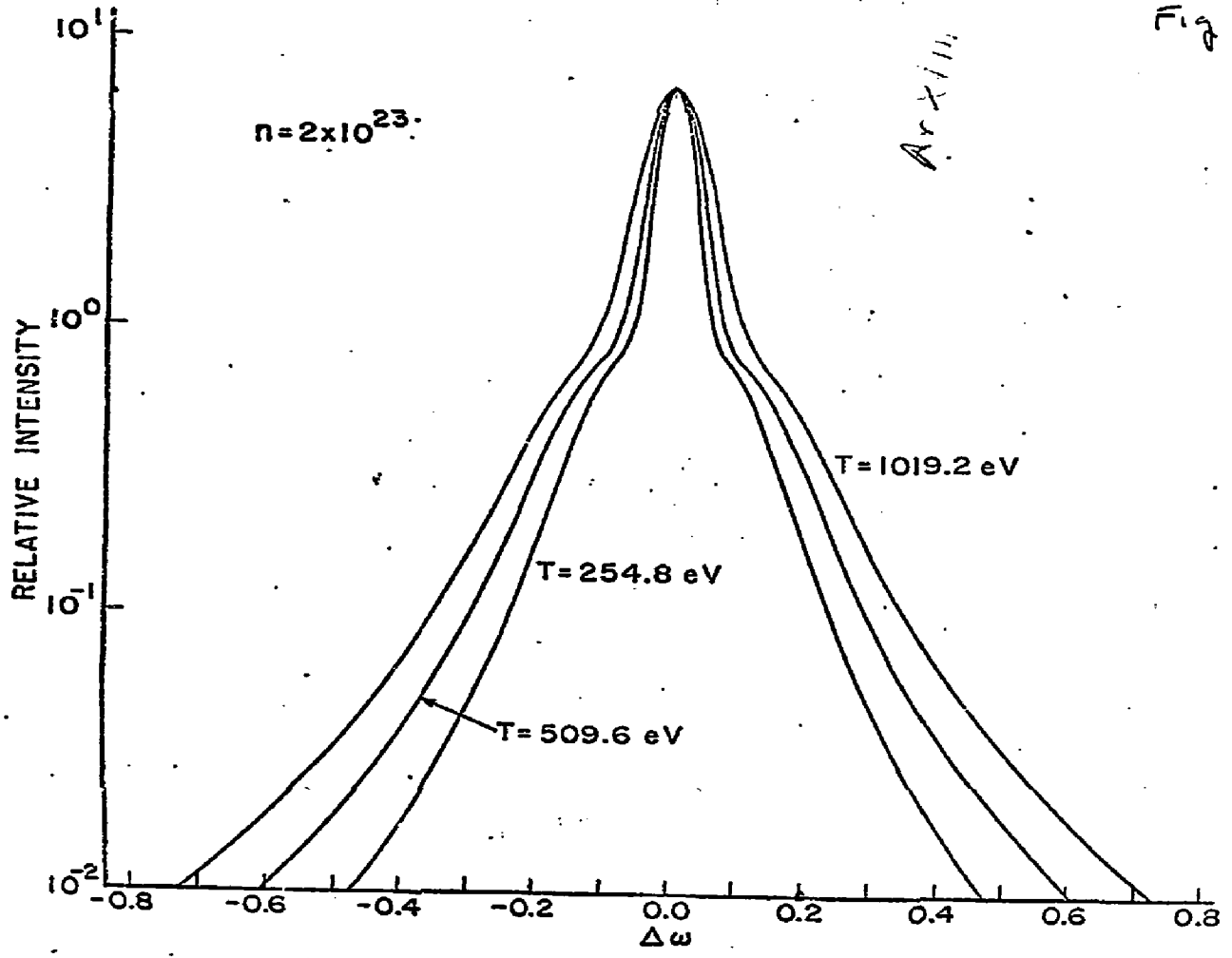
Ar XVIII
n=2x10^23
RELATIVE INTENSITY
10^1
10^0
10^-1
10^-2
T=1019.2 eV
T=254.8 eV
T=509.6 eV
-0.8
-0.6
-0.4
-0.2
0.0
0.2
0.4
0.6
0.8
Δω